Modeling Oxygen Requirements in Ischemic Cardiomyocytes

by

Anthony Drew McDougal

B.S.E., Mechanical and Aerospace Engineering
Princeton University, 2010

Submitted to the Department of Mechanical Engineering
in Partial Fulfillment of the Requirements for the Degree of

MASTER OF SCIENCE IN MECHANICAL ENGINEERING
at the
MASSACHUSETTS INSTITUTE OF TECHNOLOGY
June 2015

Signature of Author: Signature redacted
Department of Mechanical Engineering
May 8, 2015

Certified by: Signature redacted
C. Forbes Dewey, Jr.
Professor of Mechanical Engineering and Biological Engineering
Thesis Supervisor

Accepted by: Signature redacted
David E. Hardt
Professor of Mechanical Engineering
Chairman, Committee on Graduate Students

Modeling Oxygen Requirements in Ischemic Cardiomyocytes

by

Anthony Drew McDougal

Submitted to the Department of Mechanical Engineering
on May 8, 2015 in Partial Fulfillment of the
Requirements for the Degree of Master of Science in
Mechanical Engineering

Abstract

Ischemic heart disease remains a leading cause of death globally and in the US. The most common ischemic event is a heart attack, where one or more arteries are obstructed and the cardiac muscle is deprived of oxygen. Although removing the blockage and allowing reperfusion can prevent death, at the same time it can cause significant damage through "reperfusion injury." To date, there are limited methods to predict the viability of the myocardial muscle cell (myocyte) and its quantitative conditions during ischemia. Here, we explore the viability of heart cells using a model for cellular metabolism. We use this model to predict conditions that will sustain viable concentrations of adenosine triphosphate (ATP) and compare these conditions to baseline energy consumption rates.

Glycolytic metabolism is modeled using a system of coupled ordinary differential equations that describe the individual metabolic reactions that occur within the cardiac myocyte and its surrounding tissue. Over 200 conditions were simulated to characterize a range of reduced oxygen levels and ATP consumption rates. These conditions were organized according to their steady-state level of [ATP], and reveal a distinct transition region between low levels of ATP that are sustainable and depleted ATP levels that lead to cell death.

Our simulations and analysis illustrate how very low concentrations of oxygen in the extracellular tissue allow the cells to perform essential survival functions. The model contains 58 of the molecular species within the cell, so that the conditions of the cell at the time of reperfusion can be predicted. We find the oxygen level required for viability increases roughly linearly with the ATP consumption rate, and is smaller than one would have expected based on previous results. An external tissue level O_2 concentration of around 0.007 mM is sufficient to sustain cardiomyocyte viability in the absence of beating. This level of oxygen could be achieved through collateral circulation. This model of ischemia will also provide future investigations of the reperfusion process to proceed from a known metabolic and molecular state of the cardiomyocytes preceding re-oxygenation.

Thesis Supervisor: C. Forbes Dewey, Jr.
Title: Professor of Mechanical Engineering and Biological Engineering

This thesis is dedicated to those who trained me as an engineer outside of my educational studies: Jim Boyd, Koray Ozdemir, Jim Scott, Sandy Withers-Kirby, and Yin Yang. You inspired me to joyfully pursue research.

Acknowledgements

I hope you bear with my acknowledgements, because these people have borne with me, and this work is all the better for it.

Professor Dewey has my deepest gratitude for being my mentor and advisor. I am fortunate to be supported by someone with such excitement and wisdom about tackling challenges in ischemia and reperfusion. I thoroughly enjoy working with him.

Professor Stephen Payne from the University of Oxford has provided very helpful insights on the nature of ischemia and how on how to interpret results of the model. I am also glad for discussions with Professor David Sosnovik from Massachusetts General Hospital.

I sincerely appreciate the support from the Singapore-MIT Alliance, Computational and Systems Biology Program, which enabled much of my research.

I continue to be astounded (quite honestly) by my family's interest and support in all my endeavors. Most of all, my beautiful wife's love, patience, and example have motivated me to keep learning. Thank you, Juhee.

And I thank God, to whom I make the same request Francis Bacon made, to please "vouchsafe through my hands to grant new alms to the family of man."

And thank you, reader: you are now part of a critical discussion on the most dangerous disease known to humans.

-Anthony D. McDougal

May 8, 2015

Table of Contents

Background

Ischemic heart disease is the leading cause of "years of life lost" in the US [1]. Globally, ischemic heart disease was the leading cause of years of life lost in 2012 and was the most rapidly increasing cause of death during 2000-2012 [2]. Ischemia occurs when the circulation of the blood is restricted, thereby limiting the delivery of nutrients and removal of metabolic by-products. The heart can be saved by restoring blood flow using reperfusion techniques such as Percutaneous Coronary Intervention (PCI) [3]. However, even as the heart is saved, reperfusion carries the risk of damaging additional heart tissue; this damage is termed Ischemia-Reperfusion Injury (IR injury). While reperfusion techniques have substantially advanced, our understanding of IR injury and our ability to mitigate its risk is significantly lacking [4]–[7].

It is thus imperative to identify the quantitative conditions that lead to either unsustainable or jeopardized cells during ischemia. To date, a number of groups have modeled the dynamics of the heart tissue [8]–[14]. However, only Ch'en et al. model the full development of ischemia [8], while only Wu et al. represent the onset of ischemia from normal conditions (for 30 seconds) [15]. Perhaps the model by Zhou et al. [16] is the most "complete" in regards to including all of the subdomains of metabolism during ischemia: elements of glycolysis, fatty acid metabolism, the TCA cycle, and oxidative phosphorylation are included. Zhou et al. use their model to illustrate the transition from oxygenated conditions to partial deoxygenation.

Here, we build upon these efforts to present a model that describes metabolism through various levels of deoxygenation and metabolic demand. Our broad aim is to identify the precursory conditions, developed during ischemia, that leave cells susceptible to ischemia reperfusion injury. The conditions that are suspected to play a role in reperfusion injury include calcium overload, oxidative stress, mitochondrial dysfunction, and signaling cues from death proteins. These conditions develop because of a lack of energy from ATP (due to a lack of oxygen). Therefore, to understand how these conditions arise and drive reperfusion injury, we must know the metabolic condition of the cell during ischemia up to the moment of reperfusion. More specifically, we ask how a drop in oxygen affects the ATP available for cellular functions. To this end, we have developed a model of cardiomyocyte metabolism that accounts for cytoplasmic metabolism via glycolysis, mitochondrial oxidation of pyruvate, ATP buffering, and ion transport. Glycolysis and glycogenolysis are described in particular detail in order to account for anaerobic metabolism.

There currently exists a significant amount of controversy surrounding energy demand, production, and regulation in myocytes [17]. One focal aspect of this debate is the mechanism by which ATP consumption is regulated, whether by calcium, inorganic phosphate, creatine, or otherwise [18]. Rather than evaluating these possible mechanisms, we focus on understanding what ATP consumption rates are sustainable given the cardiomyocyte's resources and its method of metabolism. Using this approach, we are able to identify sets of reasonable and unreasonable outcomes for the heart cell by evaluating simulations across the entire range of possible energy demands.

We use our model and reaction parameters from the literature to simulate the time-development of cellular conditions upon the onset of hypoxia. From these representative simulations, we predict how the energy demand and availability of oxygen impact the viability of a cardiomyocyte.

Methods

We created a model of a cardiomyocyte using the Systems Biology Markup Language (SBML) [19], [20] via the CellDesigner environment [21]. Reactions were modeled as a system of ordinary differential equations and then evaluated in the CellDesigner Simulation environment.

The model contains three compartments: a cellular compartment, a compartment for the extracellular space, and a blood vessel compartment. Reactions were included to elucidate glycolysis, glycogenesis/glycogenolysis, mitochondrial oxidation of pyruvate, ATP consumption, ATP buffering, effects of ion transport on pH, and oxygen permeation across compartments. Parameters for all reactions were taken from values found reported in experiments, other computational models, or otherwise in the literature.

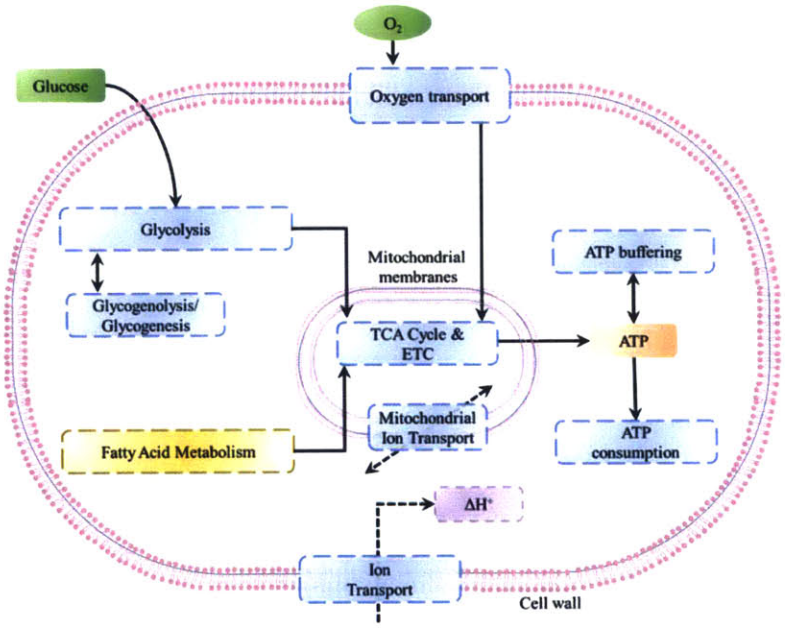

Figure 1. Overview of the metabolism components included in the model. We focus on the increased role of glycolysis during hypoxia [22], and do not explore here the role of fatty acid metabolism. All parameters are taken from the literature. Each simulation evaluates reaction using a specified fraction of available oxygen and of the ATP consumption rate.

Consistent with our goal to find how the availability of oxygen levels impacted the sustainability of energy demand, only two parameters were changed from simulation to simulation: oxygen present in the blood vessel and the percent rate of ATP consumption. In every simulation, blood vessel oxygen was set to 0.133 mM [23], and dropped to some new level after 100 sec. Simulations continued for 5000 sec, an interval that allowed all cases to reestablish a steady-state.

Over 200 trials were simulated in CellDesigner with time steps of 1 sec. The details of the model follow below.

Biochemical species

The model included 56 reactions to explicitly calculate 32 biochemical species while including the effect of other species as detailed below. The concentration of every species was recorded for all time steps. Unless otherwise indicated, concentrations refer to cellular concentrations. Extracellular concentrations are denoted with a subscript "*e*" and concentrations in the blood vessel are denoted with a subscript "*v*."

Table 1. Species evaluated in the model.

Species	*Abbreviation*	*Initial value (mM)*	*Source*
1,3-bisphosphoglycerate	13BPG	8.69×10^{-4}	[24]
2-phosphoglycerate	2PG	0.009	[24]
3-phosphoglycerate	3PG	0.071	[24]
Adenosine diphosphate	ADP	0	[8]
Adenosine monophosphate	AMP	1.00×10^{-5}	[8]*
Adenosine triphosphate	ATP	7	[8]
Bicarbonate	HCO_3^-	12.53	calculated from [25]
Bicarbonate, extracellular	$HCO_3^-{}_e$	25	[26]
Creatine	Cr	0	[8]
Creatine phosphate	CrP	25	[8]
Dihydroxyacetone phosphate	DHAP	0.036	[24]
Fructose 1,6-bisphosphate	F16BP	6.78×10^{-4}	[24]
Fructose-6-phosphate	F6P	0.041	[24]
Glucose-1,6-bisphosphate	G16BP	0.007	[24]
Glucose-1-phosphate	G1P	0.02	[24]
Glucose-6-phosphate	G6P	0.169	[24]
Glyceraldehyde-3-phosphate	GAP	0.00162	[24]
Glycerol-3-phosphate	Gly-3-P	0.158	**
Glycogen	Glg	21.4	[24]
Hydrogen	H^+	7.94×10^{-4}	[1]
Inorganic phosphate	P_i	7	[8]
Lactate	L^-	0.247	*****
Lactic Acid	LaH	155.84	*****
Myoglobin, free	Mb	0.005426	****

Myoglobin, saturated	MbO_2	0.184574	****
Oxygen (intracellular)	O_2	0.110169	***
Oxygen, extracellular	$O_{2,e}$	0.128856	***
Phosphoenolpyruvate	PEP	0.013	[24]
Pyruvate	PYR	0.055	[24]
Uridine diphosphate	UDP	0.034	[24]
Uridine diphosphate glucose	UDPG	0.099	[24]
Uridine triphosphate	UTP	0.194	[24]

Kashiwaya et al. [24] report the concentrations of metabolites found in working hearts from Wistar rats prepared with a modified Langendorff technique. The values from [1] listed here are from hearts prepared with a buffer solution containing 10mM glucose.

*Initial [AMP] is considered to be 0 by [8]. Here we have set the initial value to be a very low, negligible quantity in order to avoid a "divide by zero" error.

**Calculated from [27] and [24].

***Early iterations of the model were run with the given $[O_{2,v}]$ value, and observed to find the steady $[O_{2,e}]$ and $[O_2]$.

****[28] identifies $[Mb_{tot}]$=0.19mM. The initial values for [Mb] and [MbO] are the resulting equilibrium values given the association rates for oxygen binding (see below) and $[O_2]$

***** Calculated using the value for L^-_e and equations in [8]

Table 2. pH parameters used in the model.

Attribute	*Symbol*		*Source*
pH, cellular	pH	7.1 (initial, variable)	[1]
pH, extracellular	pH_e	7.4 (fixed)	[1]

Table 3. Species of fixed value in the model.

Fixed species	*Species*	*Initial value (mM)*	*Source*
Oxygen, in blood vessel	$O_{2,v}$	0.132593	[23]*
Oxidized nicotinamide adenine dinucleotide	NAD	2.2565	[23],[13]**
Nicotinamide adenine dinucleotide	NADH	0.7135	[23],[13]**
Lactate, extracellular	L^-_e	0.33	[29]
Glucose	Glc	1.91	[26]

*The partial pressure at the arterial entry is given by as P_1 = 100 mmHg by [23]. This is found as a concentration via $[O_{2,v}] = \alpha P_1 + Hct \times C_{Hb} \times S_{Hb}$, where $S_{Hb} = \frac{P_1^{n_H}}{P_1^{n_H} + P_{50,HB}^{n_H}}$, α =1.3×10^{-6} M mmHg^{-1}, Hct=0.45, C_{Hb}=0.0213 mol, $P_{50,Hb}$=30 mmHg, n_H=2.55.

**From [23] and later [13]: $[NAD_{tot}]$ = 2.97 = [NAD] + [NADH]. Simulations found in [13] indicate that [NADH]/[NAD] ~ 0.3 as the heart is actively regenerating ATP.

Glycolysis

All reaction values of the glycolysis pathway are taken from rat cardiomyocyte data reported by Kashiwaya et al. [24]. Reactions are generally represented as reversible Michaelis-Menten equations with modifiers from secondary reactants and products.

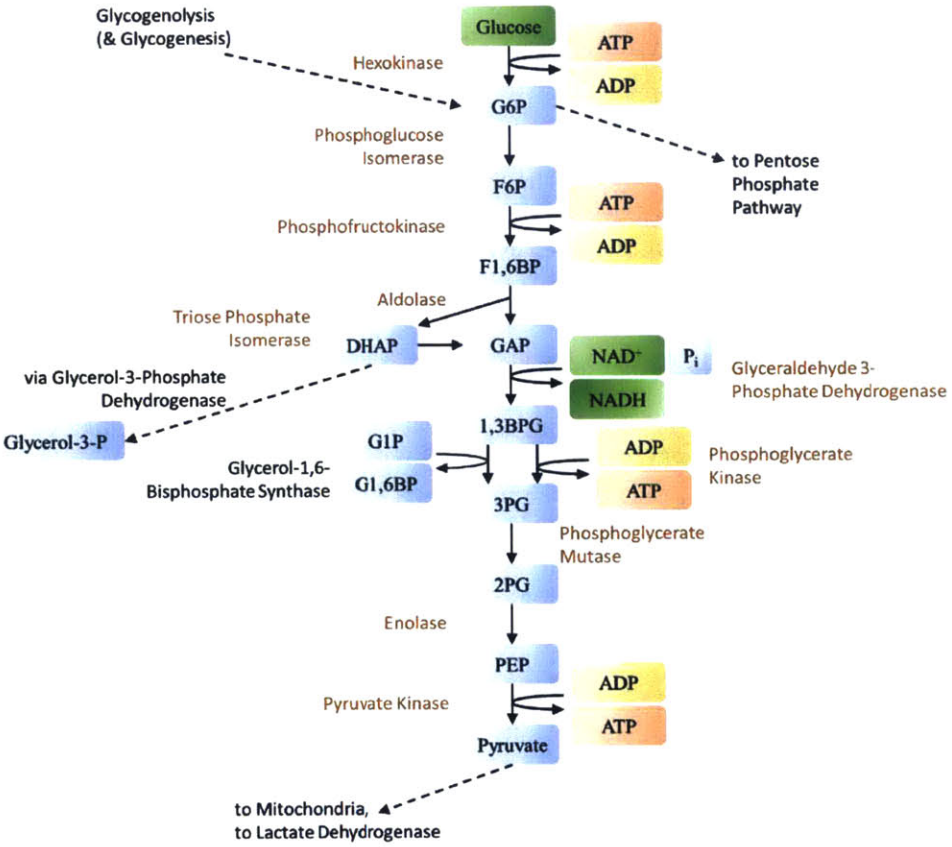

Figure 2. Reactions included in the model of glycolysis.

Hexokinase

$$Glc + ATP \rightarrow G6P + ADP + H^+ \qquad \text{(Rxn. 1)}$$

$$v_{HK} = \frac{\frac{V_{f,HK} * [Glc] * [ATP]}{K_{mf,HK}\left([ATP] + K_{HKm,ATP}\right)} - \frac{V_{r,HK} * [G6P]}{K_{mr,HK}}}{\left(1 + \frac{[Glc]}{K_{mf,HK}} + \frac{[G6P]}{K_{mr,HK}}\right)} \qquad \text{(Eq. 1)}$$

Table 4. Parameters for hexokinase.

Parameter	*Value*	*Units*	*Source*
rate of HK	푭_{HK}	mM/s	[24]
$V_{f,HK}$	0.55	mM/s	[24]
$K_{mf,HK}$	0.072	mM	[24]
$V_{r,HK}$	1.06×10^{-4}	mM/s	[24]
$K_{mr,HK}$	0.042	mM	[24]
$K_{HKm,ATP}$	0.236	mM	[24]

Phosphoglucose Isomerase

$$G6P \rightarrow F6P \qquad \text{(Rxn. 2)}$$

$$\text{푭}_{GI} = \frac{\frac{V_{f,PGI} * [G6P]}{K_{mf,PGI}} - \frac{V_{r,PGI} * [F6P]}{K_{mr,PGI}}}{\left(1 + \frac{[G6P]}{K_{mf,PGI}} + \frac{[F6P]}{K_{mr,PGI}}\right)} \qquad \text{(Eq. 2)}$$

Table 5. Parameters for phosphoglucose isomerase.

Parameter	*Value*	*Units*	*Source*
rate of PGI	푭_{GI}	mM/s	[24]
$V_{f,PGI}$	10.06667	mM/s	[24]
$K_{mf,PGI}$	0.425	mM	[24]
$V_{r,PGI}$	9.6	mM/s	[24]
$K_{mr,PGI}$	0.175	mM	[24]

Phosphofructokinase

$$F6P + ATP \rightarrow F16BP + ADP + H^+ \qquad \text{(Rxn. 3)}$$

$$\text{푭}_{FK} = \frac{\frac{V_{f,PFK} * [F6P]}{K_{mf,PFK} + [F6P]}}{\left(1 + \frac{K_{PFKM,ATP}}{[ATP]}\right)} \qquad \text{(Eq. 3)}$$

Table 6. Parameters for phosphofructokinase.

Parameter	*Value*	*Units*	*Source*
rate of PFK	v_{PFK}	mM/s	[24]
$V_{f,PFK}$	1.328333	mM/s	[24]
$K_{mf,PFK}$	0.224	mM	[24]
$K_{PFKm,ATP}$	0.127	mM	[24]

Fructose-bisphosphate Aldolase

$$F16BP \rightarrow DHAP + GAP \quad \text{(Rxn. 4)}$$

$$v_{BA} = \frac{V_{f,FBA} * [F16BP]}{K_{mf,FBA} + [F16BP]} \quad \text{(Eq. 4)}$$

Table 7. Parameters for fructose-bisphosphate aldolase.

Parameter	*Value*	*Units*	*Source*
rate of FBA	v_{BA}	mM/s	[24]
$V_{f,FBA}$	0.991667	mM/s	[24]
$K_{mf,FBA}$	0.038	mM	[24]

Triosephosphate Isomerase

$$DHAP \rightarrow GAP \quad \text{(Rxn. 5)}$$

$$v_{PI} = \frac{V_{f,TPI} * [DHAP]}{K_{mf,TPI} + [DHAP]} \quad \text{(Eq. 5)}$$

Table 8. Parameters for triosephosphate isomerase.

Parameter	*Value*	*Units*	*Source*
rate of TPI	v_{PI}	mM/s	[24]
$V_{f,TPI}$	5.933333	mM/s	[24]
$K_{mf,TPI}$	1.53	mM	[24]

Glyceraldehyde 3-Phosphate Dehydrogenase

$$GAP + NAD + P_i \rightarrow 13BPG + NADH + H^+ \quad \text{(Rxn. 6)}$$

$$\text{표}_{GAPDH} = \frac{\frac{V_{f,GAPDH} * [GAP]}{K_{mf,GAPDH} + [GAP]}}{\left(1 + \frac{K_{m,NAD^+}}{[NAD^+]}\right)} \quad \text{(Eq. 6)}$$

Table 9. Parameters for glyceraldehyde 3-phosphate dehydrogenase.

Parameter	*Value*	*Units*	*Source*
rate of GAPDH	표_{GAPDH}	mM/s	[24]*
$V_{f,GAPDH}$	5.35	mM/s	[24]
$K_{mf,GAPDH}$	0.042	mM	[24]
$K_{GAPDHm,ATP}$	0.058	mM	[24]

*$\left(1 + \frac{K_{m,Pi}}{[P_i]}\right)^{-1}$ has been omitted from this reaction, because the model does not fully track inorganic phosphate. Moreover, [8] and others illustrate how $[P_i]$ increases, driving this term from 0.83 during normal conditions toward 1 under hypoxia.

Cumulative distribution function (switch function)

A model with reactions such as ours does not account for effects at very low concentrations of substrates (and, in reversible reactions, products). One consequence of this is the possibility of calculating negative products of a particular species, indicating that the model fails at this point. Two possible strategies can handle this: 1) we stop computation when a product approaches zero, or 2) we can introduce a pseudo-term to restrict this possibility. While both slow the reaction rate to approach 0, the latter strategy allows us to observe future effects on the overall system. This approach has been used by others [8], [29] via a cumulative distribution to represent the effects of a Boltzmann distribution. One may think of it in signal terms, where a reaction is gradually "switched" off with less reacting molecules.

$$s(q) = \frac{1}{1 + e^{-\frac{[q]-a}{b}}} \quad \text{(Eq. 7)}$$

Table 10. Parameters for the cumulative distribution function.

Parameter	*Value*	*Units*	*Source*
switch function	$s_1(q)$	(unitless)	[1], [7]
[q]	current species value	mM	
a	1×10^{-4}	mM	
b	1×10^{-5}	mM	

Phosphoglycerate Kinase

$$13BPG + ADP + H^+ \rightarrow 3PG + ATP \quad \text{(Rxn. 7)}$$

$$\text{聂}_{GK} = \frac{\left(\frac{V_{f,PGK}[13BPG] * s(13BPG)}{K_{mf,PGK} * \left(1 + \frac{K_{m,ADP}}{[ADP]}\right)} - \frac{V_{r,PGK}[3PG] * s_1(3PG)}{K_{mr,PGK} * \left(1 + \frac{K_{m,ATP}}{[ATP]}\right)}\right)}{\left(1 + \frac{[13BPG]}{K_{mf,PGK}} + \frac{[3PG]}{K_{mr,PGK}}\right)} \quad \text{(Eq. 8)}$$

Table 11. Parameters for phosphoglycerate kinase.

Parameter	*Value*	*Units*	*Source*
rate of PGK	聂_{GK}	mM/s	[24]
$V_{f,PGK}$	251	mM/s	[24]
$K_{mf,PGK}$	0.021	mM	[24]
$V_{r,PGK}$	15.98333	mM/s	[24]
$K_{mr,PGK}$	0.51	mM	[24]
$K_{PGKm,ATP}$	0.008	mM	[24]
$K_{PGKm,ADP}$	0.565	mM	[24]

Phosphoglycerate Mutase

$$3PG \rightarrow 2PG \quad \text{(Rxn. 8)}$$

$$\text{聂}_{GM} = \frac{\left(\frac{V_{f,PGM}[3PG] * s_1(3PG)}{K_{mf,PGM}} - \frac{V_{r,PGM}[2PG] * s_1(2PG)}{K_{mr,PGM}}\right)}{\left(1 + \frac{[3PG]}{K_{mf,PGM}} + \frac{[2PG]}{K_{mr,PGM}}\right)} \quad \text{(Eq. 9)}$$

Table 12. Parameters for phosphoglycerate mutase.

Parameter	*Value*	*Units*	*Source*
rate of PGM	聂_{GM}	mM/s	[24]
$V_{f,PGM}$	11.23333	mM/s	[24]
$K_{mf,PGM}$	0.145	mM	[24]
$V_{r,PGM}$	48.0	mM/s	[24]
$K_{mr,PGM}$	0.139	mM	[24]

Enolase

$$2PG \rightarrow PEP + H_2O \quad \text{(Rxn. 9)}$$

$$\text{률}_{ENO} = \frac{\left(\frac{V_{f,ENO}[2PG] * s_1(2PG)}{K_{mf,ENO}} - \frac{V_{r,ENO}[PEP] * s_1(PEP)}{K_{mr,ENO}}\right)}{\left(1 + \frac{[2PG]}{K_{mf,ENO}} + \frac{[PEP]}{K_{mr,ENO}}\right)} \quad \text{(Eq. 10)}$$

Table 13. Parameters for enolase.

Parameter	*Value*	*Units*	*Source*
rate of ENO	률_{ENO}	mM/s	[24]
$V_{f,ENO}$	1.85	mM/s	[24]
$K_{mf,ENO}$	0.045	mM	[24]
$V_{r,ENO}$	2.00	mM/s	[24]
$K_{mr,ENO}$	0.089	mM	[24]

Pyruvate Kinase

$$PEP \rightarrow PYR \quad \text{(Rxn. 10)}$$

$$\text{률}_{PK} = \frac{\left(\frac{V_{f,PK}[PEP] * s_1(PEP)}{K_{mf,PK} * \left(1 + \frac{K_{PKm,ADP}}{[ADP]}\right)} - \frac{V_{r,PK}[PYR] * s_1(PYR)}{K_{mr,PK}}\right)}{\left(1 + \frac{[PEP]}{K_{mf,PK}} + \frac{[PYR]}{K_{mr,PK}}\right)} \quad \text{(Eq. 11)}$$

Table 14. Parameters for pyruvate kinase.

Parameter	*Value*	*Units*	*Source*
rate of PK	률_{PK}	mM/s	[24]
$V_{f,PK}$	9.433333	mM/s	[24]
$K_{mf,PK}$	0.11	mM	[24]
$V_{r,PK}$	0.00105	mM/s	[24]
$K_{mr,PK}$	10	mM	[24]
$K_{PKm,ADP}$	0.00268	mM	*

*[24] give $K_{PKm,ADP}$ = 0.268 mM. However, other simulations [16], [29] do not account for a K_m for ADP. We thus weakened the term due to [ADP] by decreasing $K_{PKm,ADP}$ by two orders of magnitude.

Glucose-6-Phosphate Dehydrogenase

$$G6P \rightarrow \emptyset \qquad \text{(Rxn. 11)}$$

$$v_{6PD} = \frac{V_{f,G6PD} * v_{PGI}}{v_{ss,PGI}} \qquad \text{(Eq. 12)}$$

Table 15. glucose-6-phosphate dehydrogenase.

Parameter	*Value*	*Units*	*Source*
rate of G6PD	v_{6PD}	mM/s	*
$V_{f,G6PD}$	0.095	mM/s	[24]
$v_{ss,PGI}$	0.125	mM/s	[24]

* The flux into the pentose phosphate pathway, away from G6P, is represented by G6P dehydrogenase. This flux has a maximum rate (0.0095 mM/s indicated by [24]), and is set to run at a percentage level equivalent to the percentage of maximum flux through phosphoglucose isomerase. Glycerol-3P

Glycerol-3-Phosphate Dehydrogenase

Wu et al. 1991 [30] give the parameters (but excludes the maximum reaction velocity) for a random sequential bi bi equation to calculate this flux of DHAP away from glycolysis.

$$DHAP + NADH \rightarrow Gly\text{-}3\text{-}P + NAD \qquad \text{(Rxn. 12)}$$

$$v_{3PD} = \frac{V_{f,G3PD} * [DHAP] * [NADH]}{K_{ia,NADH} * K_{m,DHAP} + K_{m,DHAP} * [NADH] + K_{m,NADH} * [DHAP] + [DHAP] * [NADH]} \qquad \text{(Eq. 13)}$$

Table 16. Parameters for glycerol-3-phosphate dehydrogenase.

Parameter	*Value*	*Units*	*Source*
rate of G3PD	v_{3PD}	mM/s	[30]
$V_{f,G3PD}$	20	mM/s	*
$K_{ia,NADH}$	0.00107	mM	[30]
$K_{m,DHAP}$	0.3	mM	[30]
$K_{m,NADH}$	0.00284	mM	[30]

*The maximum velocity was set at a value that allowed the species in glycolysis to rapidly stabilize near the values given by Kashiwaya et al. when glucose and pyruvate concentrations where held constant. The steady-state ratio of G6P and glycerol-3 phosphate from [27] are used to calculate the steady glycerol-3 phosphate level from the G6P level reported by Kashiwaya et al.

Glucose-1,6-Bisphosphate Synthase

$$13BPG + G1P \rightarrow 3PG + G16BP \quad \text{(Rxn. 13)}$$

$$\text{聂}_{BPS} = \frac{\left(\frac{V_{f,GBPS} * [13BPG]}{K_{mf,GBPS} * \left(1 + \frac{K_{m,G1P}}{[G1P]}\right)} - \frac{V_{r,GBPS} * [3PG]}{K_{mr,GBPS} * \left(1 + \frac{K_{m,G16BP}}{[G16BP]}\right)}\right)}{\left(1 + \frac{[13BPG]}{K_{mf,GBPS}} + \frac{[3PG]}{K_{mr,GBPS}}\right)} \quad \text{(Eq. 14)}$$

Table 17. Parameters for glucose-1,6-bisphosphate synthase.

Parameter	*Value*	*Units*	*Source*
rate of GBPS	聂_{GBPS}	mM/s	*
Vf,GBPS	10	mM/s	*
Kmf,GBPS	0.021	mM	*
Vr,GBPS	6	mM/s	*
Kmr,GBPS	0.51	mM	*
Km,G1P	0.008	mM	*
Km,G16BP	0.565	mM	*

* Glucose-1,6-bisphosphate synthase is an enzyme that produces G1,6BP and 3PG from G1P and 1,3BPG [31], [32]. However, to the best of our knowledge, the literature is lacking data regarding its quantitative role in specific tissues. We took steps to estimate the reaction as follows, but as this synthase becomes better understood, this model should be updated accordingly. All K_m for this reaction were treated as identical to the corresponding parameters in phosphoglycerate kinase. Because GBPS is expected to give only a minor contribution to glycolysis "parallel to" PGK, the maximum forward rate $V_{f,GBPS}$ was set to approximately 1/25 of $V_{f,PGK}$. Additionally, the ratio $V_{f,GBPS}/V_{r,GBPS}$ was approximated as $V_{f,PGM}/V_{r,PGM}$ on account of the links between PGM and GBPS [9], [10].

Glycogenesis and glycogenolysis

Phosphoglucomutase

$$G1P \rightarrow G6P \quad \text{(Rxn. 14)}$$

$$\text{聂}_{GM} = \frac{\left(\frac{V_{f,PGM} * [G1P]}{K_{mf,PGM}} - \frac{V_{r,PGM} * [G6P]}{K_{mr,PGM}}\right)}{\left(1 + \frac{[G1P]}{K_{mf,PGM}} + \frac{[G6P]}{K_{mr,PGM}}\right)} \quad \text{(Eq. 15)}$$

Table 18. Parameters for phosphoglucomutase.

Parameter	*Value*	*Units*	*Source*
rate of PGM	ν_{PGM}	mM/s	[24]
$V_{f,PGM}$	1.933	mM/s	[24]
$K_{mf,PGM}$	0.045	mM	[24]
$V_{r,PGM}$	1.12	mM/s	[24]
$K_{mr,PGM}$	0.67	mM	[24]

Inhibition by AMP

The reactions for glycolysis/glycogenolysis are (mostly) given by [24] (see following). However, in order to prevent glycogen from being relied on too soon, the cell uses AMP to inhibit glycogen phosphorylase, which can be represented [26] as

$$\left(1+\left(\frac{K_{m,AMP}}{[AMP]}\right)^{h}\right)^{-1} \quad \text{(Eq. 16)}$$

However, in order to maintain equilibrium within the glycolysis/glycogenolysis loop during perfuse conditions, our simulation required all equations to be inhibited by AMP, and so the inhibition term is included for UDP-glucose pyrophosphorylase, glycogen synthase D-form, glycogen synthase I-form, and glycogen phosphorylase. Parameters for this inhibition are given below.

Table 19. Parameters used for inhibition by AMP.

Parameter	*Value*	*Units*	*Source*
$K_{m,AMP}$	0.016	mM	[26]
h	1.5	(unitless)	[26]

UDP-Glucose Pyrophosphorylase

$$G1P + UTP + H^{+} \rightarrow UDPG + 2 \cdot P_i \quad \text{(Rxn. 15)}$$

$$\nu_{UGP} = \frac{X_{UGP}\left(k_{f,UPG} * [G1P] - k_{r,UPG} * [UDPG]\right)}{1+\left(\frac{K_{m,AMP}}{[AMP]}\right)^{h}} \quad \text{(Eq. 17)}$$

Table 20. Parameters for UDP-glucose pyrophosphorylase.

Parameter	*Value*	*Units*	*Source*
rate of UGP	v_{UGP}	mM/s	*
X_{UGP}	10000	(unitless)	*
$k_{f,UPG}$	4.36	1/s	[24]*
$k_{r,UPG}$	0.8808	1/s	[24]*
$K_{m,AMP}$	0.016	mM	[26]
h	1.5	(unitless)	[26]

*UGP is treated as working effectively at equilibrium in a fashion similar to creatine kinase above, where the magnitude of the relative rates are approximated by a large factor X. However, unlike creating kinase, we do not have the equilibrium concentrations for all the species involved in UGP. Thus we use the $K_{eq} = 4.36$ given by [24] to approximate the relative reaction rates: $K_{eq} = \frac{[UDPG]_{eq}[uknown]}{[G1P]_{eq}}$. Solving for $[unknown]$ allows us to obtain $\frac{K_{eq}}{[unknown]} = \frac{k_{f,UPG}}{k_{r,UPG}}$.

Glycogen Synthase D-form

$$UDPG \rightarrow UDP + Glg \qquad \text{(Rxn. 16)}$$

$$v_{SD} = \frac{V_{f,GSD} * [UDPG]}{\left(K_{mf,GSD} + [UDPG]\right) * \left(1 + \left(\frac{K_{m,AMP}}{[AMP]}\right)^{h}\right)} \qquad \text{(Eq. 18)}$$

Table 21. Parameters for glycogen synthase D-form.

Parameter	*Value*	*Units*	*Source*
rate of GSD	v_{SD}	mM/s	*
$V_{f,GSD}$	0.146833	mM/s	[24]
$K_{mf,GSD}$	1.42	mM	[24]
$K_{m,AMP}$	0.016	mM	[26]
h	1.5	(unitless)	[26]

Glycogen Synthase I-form

$$UDPG \rightarrow UDP + Glg \qquad \text{(Rxn. 17)}$$

$$v_{SI} = \frac{V_{f,GSI} * [UDPG]}{\left(K_{mf,GSI} + [UDPG]\right) * \left(1 + \left(\frac{K_{m,AMP}}{[AMP]}\right)^{h}\right)} \qquad \text{(Eq. 19)}$$

Table 22. Parameters for glycogen synthase I-form.

Parameter	*Value*	*Units*	*Source*
rate of GSI	률_{GSI}	mM/s	*
$V_{f,GSI}$	0.146833	mM/s	[24]
$K_{mf,GSI}$	0.08	mM	[24]
$K_{m,AMP}$	0.016	mM	[26]
h	1.5	(unitless)	[26]

Glycogen Phosphorylase

$$Glg + P_i \rightarrow G1P \qquad \text{(Rxn. 18)}$$

$$\text{률}_{GP} = \frac{\left(\frac{V_{f,GP} * [Glg]}{K_{mf,GP}} - \frac{V_{r,GP} * [G1P]}{K_{mr,GP}}\right)}{\left(1 + \frac{[Glg]}{K_{mf,GP}} + \frac{[G1P]}{K_{mr,GP}}\right) * \left(1 + \left(\frac{K_{m,AMP}}{[AMP]}\right)^{h}\right)} \qquad \text{(Eq. 20)}$$

Table 23. Parameters for glycogen phosphorylase.

Parameter	*Value*	*Units*	*Source*
rate of GP	률_{GP}	mM/s	*
$V_{f,GP}$	0.781667	mM/s	[24]
$K_{mf,GP}$	0.1	mM	[24]
$V_{r,GP}$	55.83333	mM/s	[24]
$K_{mr,GP}$	5	mM	[24]
$K_{m,AMP}$	0.016	mM	[26]
h	1.5	(unitless)	[26]

Mitochondrial oxidation of pyruvate

For this version of the model, we elected to represent the mitochondrial oxidation of pyruvate as an estimation [26], [29] since we primarily emphasize glycolysis and the reactions more heavily represented during anaerobic considerations. Equations to directly model pyruvate dehydrogenase, the citric acid cycle, electron transport chain, and related reactions and ion exchanges are included in the estimation below. Other models [10], [13], [16] consider the details of various aspects of these components, and future efforts may incorporate equations from those models.

$$15 \cdot ADP + 15 \cdot P_i + 3 \cdot O_2 + PYR + NADH \rightarrow 15 \cdot ATP + 3 \cdot CO_2 + NAD \quad \text{(Rxn. 19)}$$

$$\text{푉}_{OxP} = \text{푉}_K * \left(\frac{[ADP]}{[ADP] + K_{m,ADP}}\right) * \left(\frac{[O_2]}{[O_2] + K_{m,O2}}\right) \quad \text{(Eq. 21)}$$

Table 24. Parameters for the mitochondrial oxidation of pyruvate.

Parameter	*Value*	*Units*	*Source*
rate of OxP	푉_{OxP}	mM/s	*
$K_{m,ADP}$	5	mM	[24]
$K_{m,O2}$	0.00297	mM	[29]

*This reaction is modified from [29]. We remove their "switching function," (Eq. 7) because of its handling of ADP, which is already accounted for. Additionally, since we are abbreviating reactions following pyruvate kinase, we likewise remove the term for activation by pyruvate in this equation, instead opting to match the maximum velocity to the velocity of pyruvate generation 푉_K.

ATP consumption

As mentioned, the model uses a fixed ATP consumption rate in its simulations. We use a base ATP consumption rate as reported on beating canine experiments [15]. Each of our simulations then explore some percentage r_{atp} of this rate.

$$ATP \rightarrow ADP + P_i + H^+ \quad \text{(Rxn. 20)}$$

$$\text{푉}_{ATPase} = r_{atp} * VR_{cell,cyto} * X_{ATPase} * s_2(ATP) \quad \text{(Eq. 22)}$$

Table 25. Parameters for ATP consumption.

Parameter	*Value*	*Units*	*Source*
rate of ATPase	푉_{ATPase}	mM/s	[15]
r_{atp}	*	(unitless)	(N/A)
$VR_{cell,cyto}$	1.4703	Ratio of cellular to cytoplasmic volume	[23]
X_{ATPase}	0.39	mmol/(s · cellular liter)	[15]

* r_{atp} represents the fixed percentage of ATP consumption, which is one of the two values changed from simulation to simulation.

The s_2 function merely serves to halt this fixed consumption rate once ATP falls to an arbitrarily low value ([ATP]=0.002 mM). This function also has the form of a cumulative distribution function given above, but the parameters here allow for a sharper "switch-off" of ATP consumption.

$$s(q) = \frac{1}{1 + e^{-\frac{[q]-a}{b}}} \quad \text{(Eq. 7)}$$

Table 26. Parameters for the switch function for ATP consumption.

Parameter	*Value*	*Units*	*Source*
Switch function	$s_2(q)$	(unitless)	[1], [7]
[q]	current species value	mM	
a	1×10^{-3}	mM	
b	1×10^{-4}	mM	

ATP buffering

Two enzymes in the cytoplasm contribute to buffering ATP levels. Creatine kinase transfers a phosphate group to ADP, while adenylate kinase transfers a phosphate group from one ADP to another. Both reactions are considered to work at quasi-equilibrium when compared to the other reactions in the model, and so their reaction velocities are driven at some high value to achieve their equilibrium ratio [23].

Creatine Kinase

$$ADP + CrP + H^+ \rightarrow ATP + Cr \quad \text{(Rxn. 21)}$$

$$v_{CK} = X_{CK} * (K_{CK} * [ADP] * [CrP] * [H^+] - [ATP] * [Cr]) \quad \text{(Eq. 23)}$$

Table 27. Parameters for creatine kinase.

Parameter	*Value*	*Units*	*Source*
rate of CK	v_{CK}	mM/s	[23]
X_{CK}	10000	$mM/(s \cdot mM^2)$	[23]
K_{CK}	1660000	1/mM	[23]

Adenylate Kinase

$$2 \cdot ADP \rightarrow ATP + AMP \quad \text{(Rxn. 22)}$$

$$v_{AK} = X_{AK} * (K_{AK} * [ADP]^2 - [AMP] * [ATP]) \quad \text{(Eq. 24)}$$

Table 28. Parameters for adenylate kinase.

Parameter	*Value*	*Units*	*Source*
rate of AK	률_{AK}	mM/s	[23]
X_{AK}	10000	mM/(s · mM^2)	[23]
K_{AK}	1	(unitless)	[8]

Effects of ion transport on pH

Two equations of our model, creatine kinase (Eq. 23) and lactic acid association (Eq. 34), depend on the number of hydrogen ions available, which requires some estimation of pH in the cell.

The model incorporates a preliminary accounting of the effect that ion flow has on pH, following the approach taken by [8]. Cl^--HCO_3^- exchange (*AE*), Cl^--OH^- exchange (*CHE*), Na^+-H^+ exchange (*NHE*), and Na^+-HCO_3^- symport (*NHS*) can all be represented as functions pH:

$$J_{AE} = \frac{1}{60} \times (-15.2266606471 \times pH^4 + 302.2590169999 \times pH^3 - 1823.1533057568 \times pH^2 + 1976.4960115099 \times pH + 8383.533719598) \quad \text{(Eq. 25)}$$

$$J_{CHE} = \frac{1}{60} \times (-0.272561314 \times pH^4 + 12.313011154 \times pH^3 - 181.7704305807 \times pH^2 + 1108.6191429405 \times pH - 2422.8396631585) \quad \text{(Eq. 26)}$$

$$J_{NHE} = \frac{1}{60} \times (20.6092567224 \times pH^4 - 606.5562860276 \times pH^3 + 6701.065336577 \times pH^2 - 32930.5476482116 \times pH + 60727.9345421164) \quad \text{(Eq. 27)}$$

$$J_{NHS} = \frac{1}{60} \times (2.3290050022 \times pH^3 - 45.1765173617 \times pH^2 + 286.7706982101 \times pH - 592.1682240141) \quad \text{(Eq. 28)}$$

In addition, $[HCO_3^-]$ is estimated as per [25]:

$$[HCO_3^-] = [HCO_{3\,e}^-] \times 10^{pH - pH_e} \quad \text{(Eq. 29)}$$

Using these parameters, we can estimate the pH change [8]:

$$\frac{dpH}{dt} = \frac{-0.8 \times \text{률}_{ATPase} + 0.4 \times \text{률}_{\epsilon K} + J_{AE} + J_{CHE} + J_{NHE} + J_{NHS} - \text{률}_{LHX} + \text{률}_{LA}}{2.3 \times [HCO_3^-] - 28 \times pH + 222.6} \quad \text{(Eq. 30)}$$

$$[H^+] = 1000 \times 10^{-pH} \ (in\ mM) \qquad \text{(Eq. 31)}$$

Lactate transport, lactate dehydrogenase, and lactic acid association

Lactate affects both the pH and pyruvate levels. The presence of lactate evolves according to the following reactions.

Lactate Dehydrogenase

$$PYR + NADH + H^+ \rightarrow L^- + NAD \qquad \text{(Rxn. 23)}$$

$$\text{률}_{LDH} = \frac{V_{f,LDH} * [PYR]}{(K_{mf,LDH} + [PYR]) * \left(1 + \frac{K_{LDHm,NADH}}{[NADH]}\right)} \qquad \text{(Eq. 32)}$$

Table 29. Parameters for lactate dehydrogenase.

Parameter	*Value*	*Units*	*Source*
rate of LDH	률_{LDH}	mM/s	[24]
$V_{f,LDH}$	23.93333	mM/s	[24]
$K_{mf,LDH}$	0.125	mM	[24]
$K_{LDHm,NADH}$	0.001	mM	[24]

Lactate/H^+ Cotransporter

$$L_e^- + H_e^+ \rightarrow L^- + H^+ \qquad \text{(Rxn. 24)}$$

$$\text{률}_{HX} = \frac{V_{f,LHX} * [L_e^-]}{K_{mf,LHX} + [L_e^-]} - \frac{V_{r,LHX} * [L^-]}{K_{mr,LHX} + [L^-]} \qquad \text{(Eq. 33)}$$

Table 30. Parameters for lactate/H^+ cotransporter.

Parameter	*Value*	*Units*	*Source*
Rate of LHX	률_{HX}	mM/s	[8]
$V_{f,LHX}$	0.04817	mM/s	[8]
$K_{mf,LHX}$	2.2	mM	[8]
$V_{r,LHX}$	0.1817	mM/s	[8]
$K_{mr,LHX}$	6.92	mM	[8]

Lactic Acid Association

$$L^- + H^+ \rightarrow LaH \quad \text{(Rxn. 25)}$$

$$\text{표}_{LA} = X_{LA} * \left(\frac{[L^-] * [H^+]}{K_{LA}} - [LaH] \right) \quad \text{(Eq. 34)}$$

Table 31. Parameters for lactic acid association.

Parameter	*Value*	*Units*	*Source*
rate of LA	표_{LA}	mM/s	[8]
K_{LA}	1.259×10^{-7}	mM	[8]
X_{LA}	10000	1/s	[8]

Oxygen permeation across compartments

Oxygen transport is modeled as a description of membrane permeability across three compartments. The value of oxygen for the blood vessel compartment is held fixed and allows the oxygen to enter new compartments, each of which is approximated as being well-mixed.

Permeation of O_2 (vessel-extracellular)

$$O_{2,V} \rightarrow O_{2,E} \quad \text{(Rxn. 26)}$$

$$\text{표}_{O_2VE} = \frac{PA_{VE}}{V_e}([O_{2,v}] - [O_{2,e}]) \quad \text{(Eq. 35)}$$

Table 32. Parameters for oxygen transport from blood vessel to extracellular compartment.

Parameter	*Value*	*Units*	*Source*
Rate of O_2VE	표_{O_2VE}	mM/s	[23]
PA	50	L/s	[23]
V_e	0.241/0.0684	1	[23]

*SBML automatically handles volume sizes across compartments by calculating total amount of substance crossed, that is, concentration time an implicit compartment volume; we have added the ratio of the compartments here for ease of reading. [23] gives the relative volumes of each compartment. Calculating these relative to the cytoplasm, we have $V_{extracellular}/V_{cytoplasm} = 0.241$ and $V_{vessel}/V_{cytoplasm} = 0.0684$.

Permeation of O_2 (Extracellular-cellular)

$$O_{2,E} \rightarrow O_{2,C} \quad \text{(Rxn. 27)}$$

$$v_{O_2EC} = \frac{PA_{EC}}{V_c}([O_{2,e}] - [O_{2,c}]) \quad \text{(Eq. 36)}$$

Table 33. Parameters for oxygen transport from extracellular compartment to cellular compartment.

Parameter	*Value*	*Units*	*Source*
rate of O_2EC	v_{O_2EC}	mM/s	[23]
PA	10	L/s	[23]
*V_c	1/0.241	1	[23]

*As above, SBML automatically handles volume sizes across compartments. The relative volume $V_{extracellular}/V_{cytoplasm} = 0.241$ is determined from values given in [23].

Myoglobin-oxygen binding

While the dynamics for myoglobin-enhanced transport are on a fast time scale for the results in this model, they are nonetheless incorporated to facilitate future simulations [28].

$$Mb + O_2 \rightarrow MbO_2 \quad \text{(Rxn. 28)}$$

$$v_{MB} = k_a * [Mb] * [O_2] - k_d * [MbO_2] \quad \text{(Eq. 37)}$$

Table 34. Parameters for myoglobin binding to oxygen.

Parameter	*Value*	*Units*	*Source*
rate of MB	v_{MB}	mM/s	[28]
k_a	15400	1/(mM · s)	[28]
k_b	60	1/s	[28]

Results

The simulations predict the metabolic behavior of the cardiomyocyte upon hypoxia. Once the level of blood oxygen is lowered, the concentration of ATP is maintained by a sequence of three energy buffers: we observe a drop in creatine phosphate, followed by the fall of glycogen, and finally a rise in AMP as ADP is sacrificed. Throughout these events, the reactions of glycolysis are providing an anaerobic source of ATP. Figure 3 illustrates the response to deoxygenation after a brief period of stable, oxygenated conditions. In comparison to [ATP] falling to 0 on the order of 550 sec, Ch'en et al. used a completely anaerobic model [8] and found [ATP] to last roughly 800 sec. Wu et al. [15] provide another point of comparison regarding CrP: when totally occluding canine coronary blood flow, CrP fell to 10 mM in 35 seconds; our simulations take 110 seconds to show the same change, but under incomplete occlusion. Overall, the model simulations are of the same scale as other simulations and experiments in the literature.

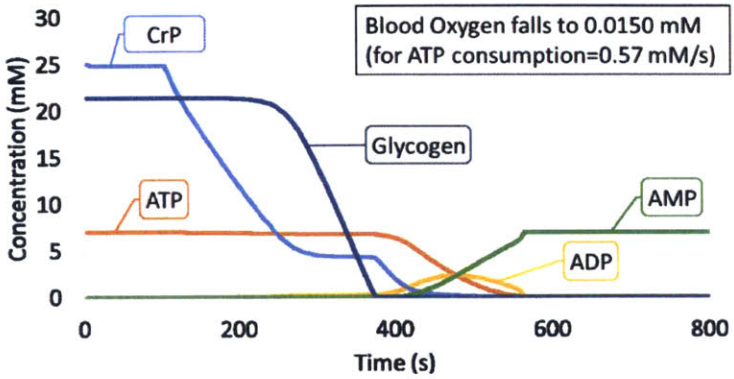

Figure 3. Metabolite response to deoxygenation in an example simulation of the model. r_{atp} = 100%, leading to constant ATP consumption rate of 0.57 mM/s. At the outset, $[O_{2,V}]$ = 0.13 mM and the system stays at steady-state. After 100s, $[O_{2,V}]$ falls to some fraction (here, 0.015 mM).

If the oxygen supply is decreased to an even lower value, the rate of mitochondrial oxidation of pyruvate is further decreased, further hampering the greatest energy source. Consequently, the energy buffers will deplete faster in an effort to keep [ATP] at high levels, and the cell will crash more rapidly. Conversely, if the oxygen is slightly increased, mitochondrial reactions are able to provide more energy to supplement anaerobic metabolism, which lessens the pull on the buffers and extends the survival of the cell (by a similar token, a variable ATP consumption rate will likely change the time to ATP depletion; this is explored further in the *Discussion* below).

After the transient behavior of the system, we see that the final outcome of each simulation is determined by the amount of oxygen available and the amount of ATP being consumed. If the oxygen level is sufficiently increased, the concentration of ATP shows no perceptible change. However, there is a transition range of oxygen concentrations that lead to an intermediate steady-state level of [ATP] (see Figure 4). Thus we see that, for a specified ATP consumption rate, lowering oxygen can affect the steady levels of ATP—resulting in catastrophically low concentrations at some O_2 level. From a metabolic standpoint, the cell cannot continue to live without ATP providing energy for fundamental functions.

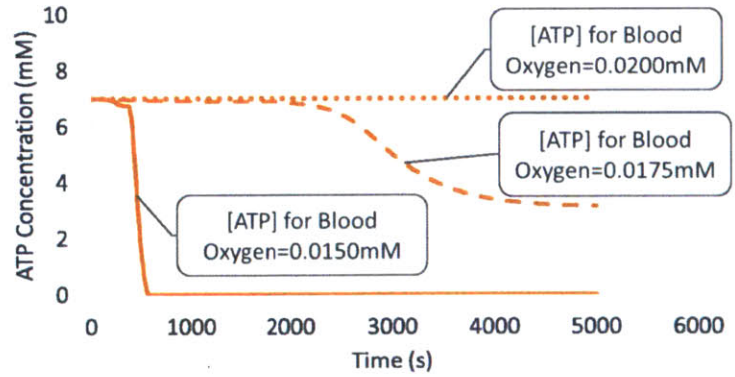

Figure 4. Comparison of ATP trends for various changes to the blood vessel oxygen. Solid line, $[O_{2,V}]$ falls to 0.0150mM, identical to Figure 3. Dashed line, $[O_{2,V}]$ falls to 0.0200mM. Dotted line, $[O_{2,V}]$ falls to 0.0200mM.

Yet [ATP] never reaches zero; thus, we must define some lower threshold of [ATP] in order to compare the outcome of various simulation conditions. One possible threshold would be concentrations of [ATP] sufficiently low such that the reaction rate equations are no longer representative of the chemical Langevin equations, at which point the model would overestimate the amount of ATP immediately available for consumption (thus making a fixed consumption rate unsustainable). To do this would require ATP concentrations on the order of 1×10^{-7} mM. However, to facilitate the simulation we look for cases where the ATP concentration is on the order of 1×10^{-3} mM at steady state, we identify the lower threshold of [ATP] for a sustainable fixed consumption rate to be 0.007mM, or 0.1% that of the initial [ATP] (=7mM). Conversely, we define "imperceptible changes" as reducing [ATP] to no less than 99.9% of 7mM.

We iterated our model to find all the combinations of $[O_2]$ and ATP consumption that lead to these [ATP] thresholds. The results of these simulations are plotted in Figure 5.

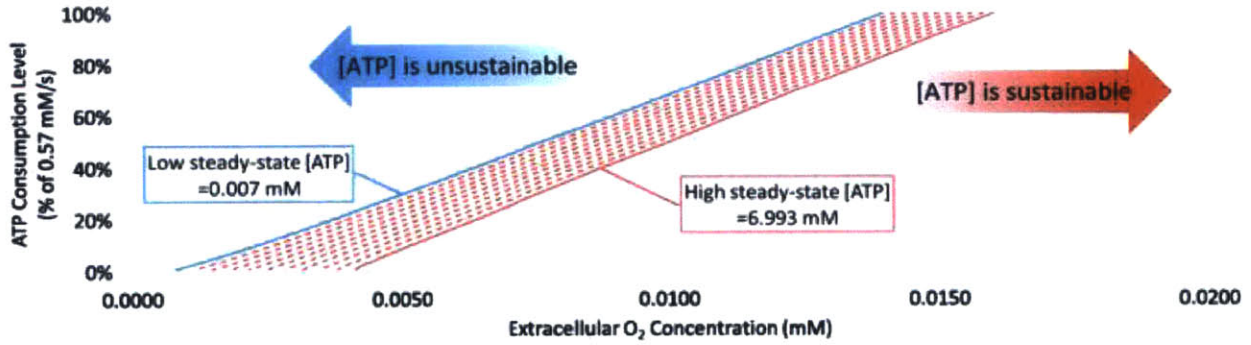

Figure 5. Curves of steady-state ATP concentration, arising from ATP consumption and extracellular oxygen. Simulations were run over all ATP consumption rates and oxygen concentrations. For this graph, although the blood vessel oxygen continues to be the simulation input, we plot the extracellular oxygen to emphasize the oxygen available in the tissue.

Solid red line: those consumption rates and $[O_{2,V}]$ that led to a steady state of [ATP] equal to 99.9% of the original ATP. Solid blue line: those consumption rates and $[O_{2,V}]$ that led to a steady state of [ATP] equal to 0.1% of the original ATP. The ATP data for the 100% ATP consumption level are found in Figure 4. Dashed red lines: range of conditions that lead to intermediate [ATP] at steady-state.

In the right-hand region of Figure 5, [ATP] shows practically no change from the original levels, and so from a metabolic standpoint, the oxygen supply and energy demand result in a sustainable state for the tissue. In the left-hand region, [ATP] is at such low levels that even the slightest increase of ATP consumption or the slightest decrease of O_2 will cause [ATP] to be insufficient. In the middle region, we see a thin range of oxygen concentrations that represent the intermediate transition from sustainable to unsustainable conditions. This "metabolic twilight" region neither exhausts ATP nor maintains it at normal levels.

Given this map, we can begin to identify some parameters that are key for the survival of the cardiomyocyte. Das and Harris [33] analyzed the energy consumed by rat cardiomyocytes under stimulation. Unstimulated, non-contracting cells were found to consume 3.7 μmol ATP/min/mg. Cells that were stimulated were found to have an increasing amount of ATP consumption, plateauing at 6.6 μmol ATP/min/mg. Thus, Das and Harris indicate that a non-contracting cell consumes 56% of the energy that a contracting cell consumes (see Figure 6).

Rolfe and Brown [34] provide a review investigating the allocation of energy among various cellular processes. These are summarized in Figure 7. Using their compiled values, we can consider that 79% of energy is directed toward contraction, while 21% is directed toward "cellular maintenance."

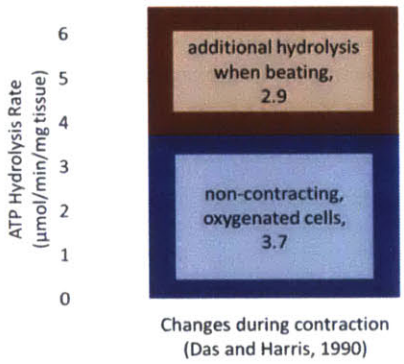

Figure 6. Energy consumed by rat heart, summary of data found in Das and Harris, 1990 [33]. Non-contracting oxygenated cells were found to expend an additional 79% when stimulated to contract.

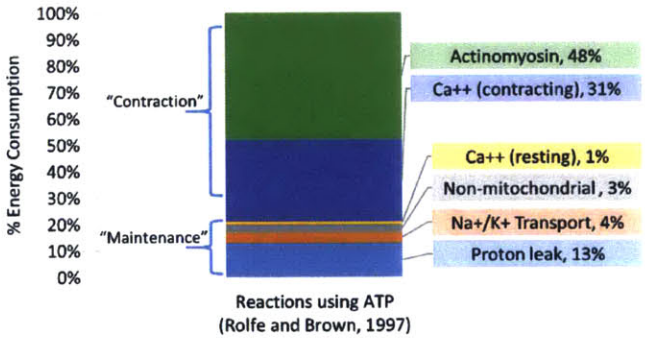

Figure 7. Energy consumed by rat heart, summary of data found in Rolfe and Brown, 1997 [34]. The values reported in that work are given as ranges; the values shown here are a proportional distribution of those values. They estimate that activities associated with contraction make up about roughly 79% of energy consumption, while activities necessary for cellular maintenance lead to 21%.

From these estimates, we can define the range of oxygen that might possibly sustain cardiomyocytes, allowing us to determine the cells that are targeted during reperfusion. When we compare Figure 5 to Figure 6 and Figure 7, we can conjecture that a baseline of somewhere in the range of 0.004-0.010 mM of oxygen is required to minimally support a cardiomyocyte.

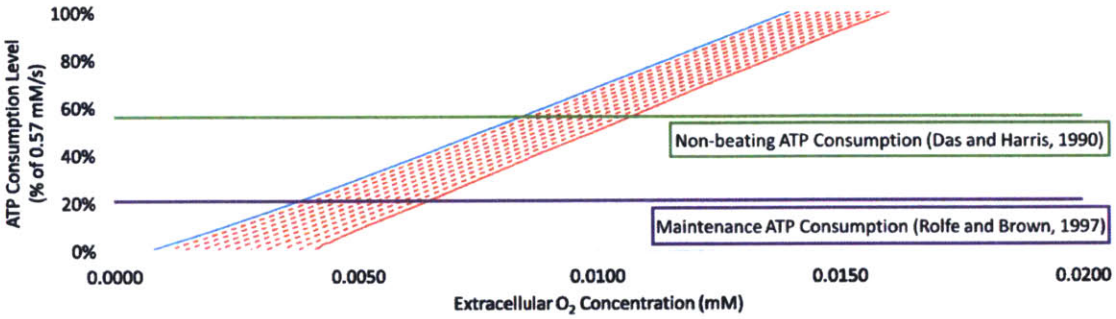

Figure 8. A comparison of the results from Figure 5, Figure 6, and Figure 7. By comparing the results from the model simulations with the percent of energy consumption required to, we can estimate that something on the order of 0.005-0.010 mM of extracellular oxygen is necessary to sustain the heart cell.

The model can be used to explore other aspects apart from our main question regarding the oxygen required to sustain [ATP]. For the remainder of this section, we illustrate one such observation. When Figure 5 is recreated using the steady-state intracellular oxygen concentration, a surprising feature is found. The cellular oxygen concentration corresponding to our high threshold of [ATP] *is lower than* the oxygen concentration that corresponds to our low threshold of [ATP] (Figure 9).

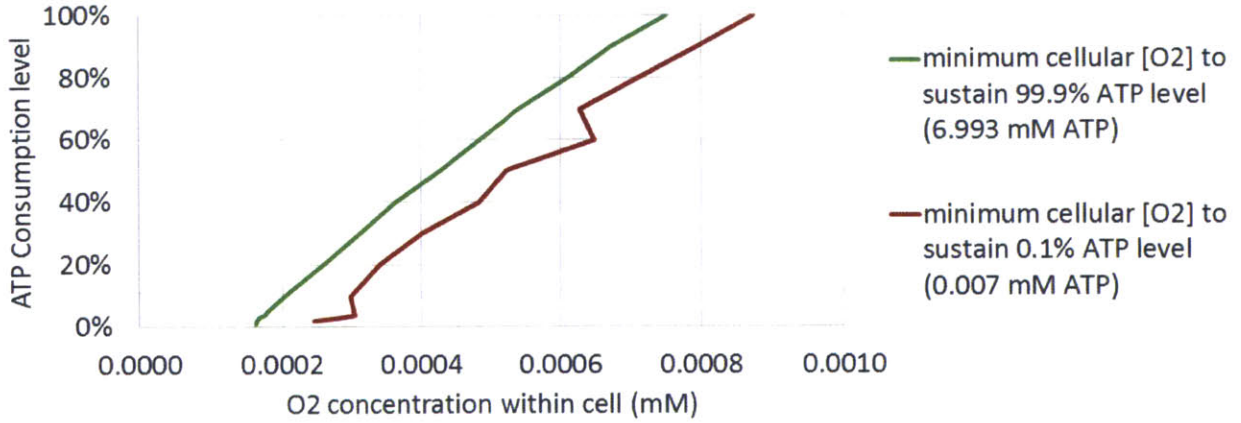

Figure 9. Cellular oxygen required to sustain ATP consumption rates. The same conditions as for Figure 5 are identified, but instead reporting cellular oxygen levels. The model reveals that intracellular levels of oxygen are higher in simulations that result in the lower threshold level of steady-state ATP.

To investigate, we compare the simulations at the 50% ATP consumption level. Figure 10 shows the reactions consuming and producing ATP within the glycolytic pathway. The "high threshold" simulation shows relatively minor changes to the creation and consumption of ATP. For the "low threshold" case, the cell keeps its ATP level afloat during the first ~1000 seconds. Ultimately, however, all reactions producing or using ATP settle to a lower rate than the corresponding reactions in the high threshold simulation. Most importantly, the mitochondrial oxidation of pyruvate is significantly lower in the case that yields [ATP]=0.007 mM, implying that less oxygen is consumed.

Figure 11 further illustrates this point. For cases with sufficiently low incoming oxygen, we see that less oxygen is consumed, ultimately causing the oxygen within the cell to rebound slightly. One may wish to look for implications this rebound has for creating reactive oxygen species, or of allowing neighboring cells to receive a slim amount of extra oxygen. However, these speculations only serve as points of departure for further experiments to probe the various observations gleaned from by the model.

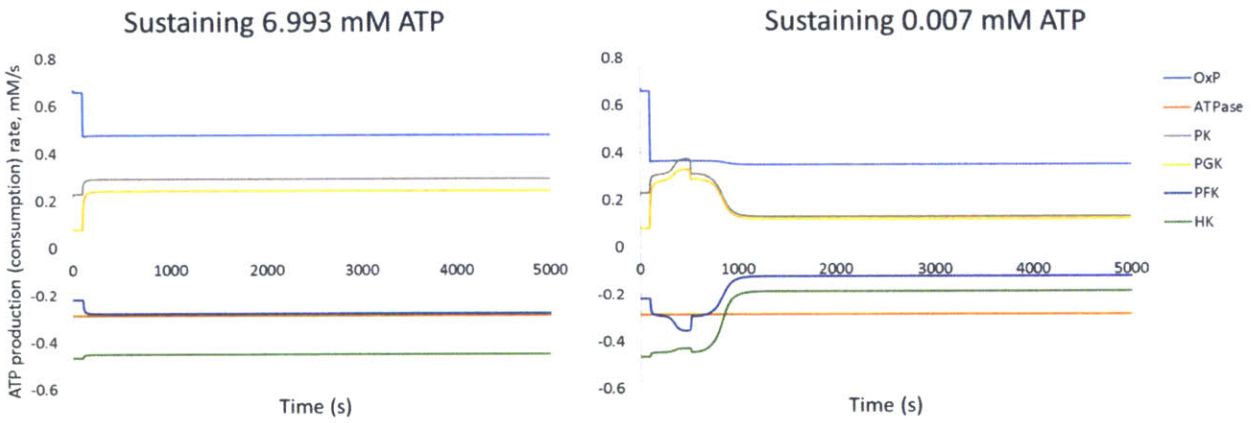

Figure 10. Reactions producing and utilizing ATP (simulations shown for at 50% ATP consumption rate). Positive rates are producing ATP, negative rates are consuming ATP. In the case leading to the high [ATP] threshold, *left*, the reaction velocities are quickly established and stabilize relatively near their values during full perfusion (during the first 100 sec). In the case leading to the low [ATP] threshold, *right*, the magnitude of all reaction velocities fall after buffer systems fall and anaerobic metabolism is established.

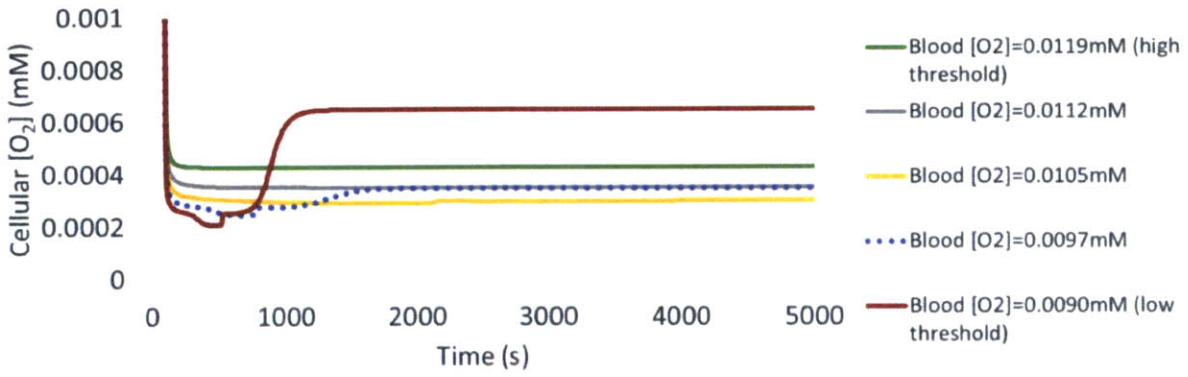

Figure 11. Intracellular oxygen values (simulations shown for at 50% ATP consumption rate). With less oxygen in the blood vessel, the amount of oxygen consumed by mitochondrial oxidation of pyruvate lessens. Eventually, the ATP buffers are depleted and the cell slows mitochondrial oxidation.

These simulation results suggest that the cell can balance energy demands using different reactions to different extents. With less oxygen, mitochondrial oxidation of pyruvate is slowed (at 100 seconds), decreasing the amount of ATP. Over the next 800 seconds, the buffers all attempt to keep the adenosine pool shifted toward ATP as much as possible. During this time, the glycolytic reactions are frequently changing velocities, but once the buffers are exhausted, these

reactions come to an equilibrium that slightly decreases the velocity of mitochondrial oxidation. Consequently, less oxygen is being consumed, resulting in the observed rise of intracellular oxygen. Interestingly, the cell uses its buffers despite the fact that it is ultimately able to match ATP supply and demand without the buffers. In effect, it appears that the cell has various combinations of reaction rates that can match ATP supply and demand. However, the system is such that if the supply of ATP is suddenly hampered, the ATP buffers are activated before the cell finds its new steady conditions.

Discussion

Our model allows us to observe the state of the cell as a result of blood oxygen concentration and specified energy demands. By identifying the conditions that yield high and low thresholds of [ATP], and comparing these conditions with the known energy needs of the cell, we are able to predict the metabolic outcome of a cell. Even with extracellular oxygen as low as 0.0160 mM (corresponding to 0.0128 mmHg), the cardiomyocyte's glycolytic pathway can provide energy required for normal cellular function, with no severe change in the cell's state. This is compatible with other reported calculations that show how extracellular pO_2 decreases along the length of a capillary until it reaches about 20 mmHg [23].

On the other hand, for a given energy level, a drop of about 0.0015 mM O_2 results in an almost negligible ATP concentration, which can represent a lower bound of oxygen that allows cells to survive. Others [35], [36] have suggested that low ATP is not correlated to cell death. However, the conditions for these claims suggest present [ATP] still within the intermediate "twilight" range, rather than a truly unsustainable concentration. For example, [36] were observing [ATP] as low as around 3% of normal [ATP], compared to our value of 0.1%. Only at the lower value will a slightly increased demand for energy become too much for ATP regeneration to keep pace, resulting in a breakdown of the cell's necessary functions. Over long durations, this breakdown will certainly cause irreversible damage (Murphy and Steenbergen also allude to this [35]).

The "metabolic twilight" of cells transitioning from high to low [ATP] is occurs over a range of 0.0015 mM O_2. We suggest that it is primarily the cells in this "transition region" that are being saved by reperfusion and, therefore, they are also the cells susceptible to reperfusion injury. At first glance, the range of $[O_2]$ that can effect an intermediate level seems far too thin to be physiologically discernable. Yet in fact, the reaction-diffusion curve covers substantial spatial distances for relatively small ranges of oxygen, after an initial region of sharp decay (see Figure 12 for an illustrative drawing). Popel and others have described how to solve the reaction-diffusion equation for various contexts [37]. Our simulations could be employed as the basis for numerical integration of the oxygen consumption with the equation.

During ischemia *in vivo*, the source of oxygen from neighboring tissue may be augmented by anastomosis. This will shift the diffusion curve in Figure 12 to the right, increasing the amount of tissue with favorable outcome. Humans have among the highest attainable coronary collateral flow, which is key in clinical cases [38]. Our simulations serve to further emphasize the importance of collateral circulation by demonstrating the value of even miniscule increases in the amount of oxygen. If the oxygen being supplied by collateral circulation is sufficiently high, cardiomyocytes may even be able to remain above the high [ATP] threshold and thereby reduce their risk of reperfusion injury. It may be worthwhile to

point out that animals generally have lower collateral flow, and thus may have tissue skewed toward a higher risk of reperfusion injury compared to human tissue; one must take care in accounting for these differences in any spatial diffusion model of the heart.

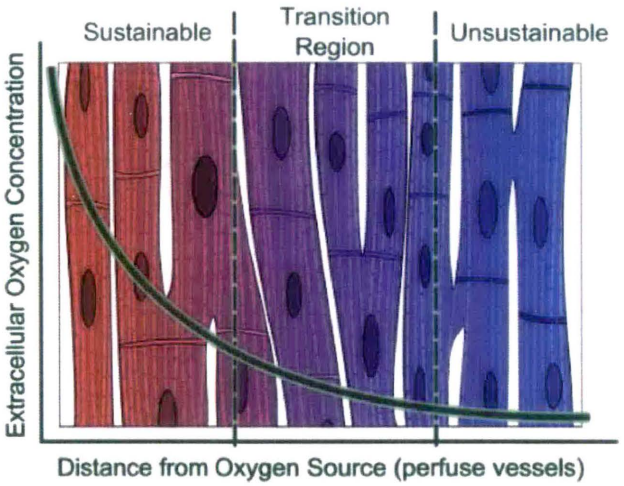

Figure 12. Hypothetical diffusion-reaction curve showing the one-dimensional decay of oxygen as a function of distance from an oxygen source. At lower levels, oxygen decays less rapidly. Consequently, even over significant distances in the tissue we may see small variations in the extracellular oxygen concentration.

While our model focuses on the metabolic viability of the cell, the lack of O_2 and the shortage of ATP and will lead to other reactions that are involved in cellular death or cellular protection beyond the basic metabolic requirements. Below, we focus on just two components that contribute further injury after the fall of glycolysis.

One factor that is key in considering IR injury is the rapid generation of reactive oxygen species [5], [35], [39]. Recent studies [40] tend to focus on the condition of the electron transport chain as the cause for increased ROS. The role of antioxidants during reperfusion remain unclear, especially for SOD: heart outcomes appear to improve with increased activity of SOD [41], [42] as well as with administered antioxidants [43]; yet SOD appears to degrade quickly when administered intravenously [44], and the level of activity SOD throughout reperfusion remains unclear [45]. However, given the exhausted supply of ATP upon reperfusion, it seems feasible that the absence of ATP available for enzyme production would lead to reduced activity of SOD, allowing ROS formation to be unchecked [46]. To be sure, there are other factors driving antioxidant maintenance in the cell, but our emphasis here is to call attention to the condition of the cell as it responds to its metabolic capacity.

Additionally, the rate of production of reactive oxygen species is dependent on both the concentration of oxygen as well as the availability of reducing agents, that is, the unused electron transport chain [47]–[49]. As Figure 11 shows, the intracellular level of oxygen increases with sufficiently low levels of [ATP] (arising from sufficiently low levels of blood oxygen). Ischemic cells can have as much as double the concentration of intracellular oxygen—and thus higher ROS production—compared to their neighbors with slightly higher oxygen concentrations.

Another important player in both ischemia and IR injury is the calcium gradient across the mitochondria. For example, Ca^{2+}-ATPase pumps will weaken as ATP is decreased [50]. In

turn, the calcium reduces the amount of ATP that can be produced, effectively trapping the cell's energy production and accelerating the death of the cell.

However, one should note that the simulations presented here are forced to a fixed ATP consumption rate rather than a variable ATP consumption rate, as might be expected in the real case. Consequently, the simulation time to ATP depletion may be shortened compared to the expected physiological case, in which decreasing [ATP] and other factors are believed to reduce the overall rate of ATP hydrolysis. As mentioned previously, a major challenge in modeling cardiomyocytes arises from the debate on how to specify ATP consumption rates as functions of metabolite concentrations [17], [18]. By representing ATP consumption as a function of metabolites in the cytoplasm, as is commonly done, one can deterministically simulate the cell's final state for a given amount of oxygen. This outcome will necessarily vary according to the model chosen for ATP consumption. Yet by fixing the ATP hydrolysis rate to a different level in each simulation, as we have done here, we are able to map all possibilities of how both the energy demand and the oxygen availability impact the final steady concentrations of the cell.

Doubtless, the model presented here will benefit from continued development. We have set some concentrations to be constant during the onset of ischemia, when they are certainly changing. Included among these are NADH, pH, and pathways branching away from glycolysis, [8], [10], [13], [26], [51]. One example of the effect of this contant is demonstrated by Vinnakota et al. as they explore the role of pH in the context of glycogenolysis. They show how accounting for variation of the pH does affect the buildup of byproducts by around 30%, yet demonstrate the same trend [51].

Additionally, while our model offers detail on glycolysis, other models emphasize details in other aspects of metabolism, such as the tricarboxylic acid cycle and the electron transport chain. A complete understanding of metabolism during extreme conditions will depend on simultaneous integration of the strengths of each of these models [52]. Our hope is that the strength of each of these models can be incorporated to provide a more complete picture of the evolution of conditions within the cell.

In conclusion, our model captures the transition from aerobic to anaerobic glycolytic metabolism, using a wide range of ATP consumption rates to predict the concentrations of biochemical species. From these, we can compute oxygen necessary to sustain ATP concentration levels. These conditions can be used to predict which cells are irrecoverable, which cells can continue normal cell function, and which cells are jeopardized yet potentially rescuable. The simulations also reveal changes in cellular conditions, such as increased intracellular O_2, that may be driving other harmful reactions.

An understanding of the quantitative conditions that drive the mechanisms of IR injury is critical for developing effective and consistent strategies for salvaging tissue. The simulations we have presented reveal a window of conditions that cause cells to enter a "metabolic twilight." It is the cardiomyocytes in this twilight zone that are susceptible to the changing environment of the cell, and their behavior will be key to understanding the character of reperfusion injury.

References

[1] US Burden of Disease Collaborators, "The state of US health, 1990-2010: Burden of diseases, injuries, and risk factors," *JAMA*, vol. 310, no. 6, pp. 591–606, Aug. 2013.

[2] World Health Organization, *World health statistics 2014.* [S.l.]: World Health Organization, 2014.
[3] D. M. Yellon and D. J. Hausenloy, "Myocardial reperfusion injury," *N. Engl. J. Med.*, vol. 357, no. 11, pp. 1121–1135, 2007.
[4] D. J. Hausenloy and D. M. Yellon, "Myocardial ischemia-reperfusion injury: a neglected therapeutic target," *J. Clin. Invest.*, vol. 123, no. 1, pp. 92–100, Jan. 2013.
[5] T. Kalogeris, C. P. Baines, M. Krenz, and R. J. Korthuis, "Cell Biology of Ischemia/Reperfusion Injury," in *International Review of Cell and Molecular Biology*, vol. 298, Elsevier, 2012, pp. 229–317.
[6] L. Schwartz Longacre, R. A. Kloner, A. E. Arai, C. P. Baines, R. Bolli, E. Braunwald, J. Downey, R. J. Gibbons, R. A. Gottlieb, G. Heusch, R. B. Jennings, D. J. Lefer, R. M. Mentzer, E. Murphy, M. Ovize, P. Ping, K. Przyklenk, M. N. Sack, R. S. Vander Heide, J. Vinten-Johansen, and D. M. Yellon, "New Horizons in Cardioprotection: Recommendations From the 2010 National Heart, Lung, and Blood Institute Workshop," *Circulation*, vol. 124, no. 10, pp. 1172–1179, Sep. 2011.
[7] P. Ferdinandy, D. J. Hausenloy, G. Heusch, G. F. Baxter, and R. Schulz, "Interaction of Risk Factors, Comorbidities, and Comedications with Ischemia/Reperfusion Injury and Cardioprotection by Preconditioning, Postconditioning, and Remote Conditioning," *Pharmacol. Rev.*, vol. 66, no. 4, pp. 1142–1174, Oct. 2014.
[8] F. F.-T. Ch'en, R. D. Vaughan-Jones, K. Clarke, and D. Noble, "Modelling myocardial ischaemia and reperfusion," *Prog. Biophys. Mol. Biol.*, vol. 69, no. 2–3, pp. 515–538, Mar. 1998.
[9] S. Cortassa, M. A. Aon, B. O'Rourke, R. Jacques, H.-J. Tseng, E. Marban, and R. L. Winslow, "A Computational Model Integrating Electrophysiology, Contraction, and Mitochondrial Bioenergetics in the Ventricular Myocyte," *Biophys. J.*, vol. 91, no. 4, pp. 1564–1589, Aug. 2006.
[10] L. D. Gauthier, J. L. Greenstein, S. Cortassa, B. O'Rourke, and R. L. Winslow, "A Computational Model of Reactive Oxygen Species and Redox Balance in Cardiac Mitochondria," *Biophys. J.*, vol. 105, no. 4, pp. 1045–1056, Aug. 2013.
[11] B. Korzeniewski, A. Noma, and S. Matsuoka, "Regulation of oxidative phosphorylation in intact mammalian heart in vivo," *Biophys. Chem.*, vol. 116, no. 2, pp. 145–157, Jul. 2005.
[12] K. Tepp, N. Timohhina, V. Chekulayev, I. Shevchuk, T. Kaambre, and V. Saks, "Metabolic control analysis of integrated energy metabolism in permeabilized cardiomyocytes—Experimental study," *Acta Biochim. Pol.*, vol. 57, no. 4, p. 421, 2010.
[13] F. Wu, F. Yang, K. C. Vinnakota, and D. A. Beard, "Computer Modeling of Mitochondrial Tricarboxylic Acid Cycle, Oxidative Phosphorylation, Metabolite Transport, and Electrophysiology," *J. Biol. Chem.*, vol. 282, no. 34, pp. 24525–24537, Aug. 2007.
[14] Y. Yaniv, W. C. Stanley, G. M. Saidel, M. E. Cabrera, and A. Landesberg, "The Role of Ca2+ in Coupling Cardiac Metabolism with Regulation of Contraction," *Ann. N. Y. Acad. Sci.*, vol. 1123, no. 1, pp. 69–78, Mar. 2008.
[15] F. Wu, E. Y. Zhang, J. Zhang, R. J. Bache, and D. A. Beard, "Phosphate metabolite concentrations and ATP hydrolysis potential in normal and ischaemic hearts," *J. Physiol.*, vol. 586, no. 17, pp. 4193–4208, Sep. 2008.
[16] L. Zhou, J. E. Salem, G. M. Saidel, W. C. Stanley, and M. E. Cabrera, "Mechanistic model of cardiac energy metabolism predicts localization of glycolysis to cytosolic subdomain

during ischemia," *Am. J. Physiol. - Heart Circ. Physiol.*, vol. 288, no. 5, pp. H2400–H2411, May 2005.
[17] M. A. Aon and S. Cortassa, "Mitochondrial network energetics in the heart," *Wiley Interdiscip. Rev. Syst. Biol. Med.*, vol. 4, no. 6, pp. 599–613, Nov. 2012.
[18] Y. Yaniv, M. Juhaszova, H. B. Nuss, S. Wang, D. B. Zorov, E. G. Lakatta, and S. J. Sollott, "Matching ATP supply and demand in mammalian heart," *Ann. N. Y. Acad. Sci.*, vol. 1188, no. 1, pp. 133–142, 2010.
[19] A. Finney and M. Hucka, "Systems biology markup language: Level 2 and beyond," *Biochem. Soc. Trans.*, vol. 31, no. 6, pp. 1472–1473, 2003.
[20] M. Hucka, A. Finney, H. M. Sauro, H. Bolouri, J. C. Doyle, H. Kitano, A. P. Arkin, B. J. Bornstein, D. Bray, A. Cornish-Bowden, A. A. Cuellar, S. Dronov, E. D. Gilles, M. Ginkel, V. Gor, I. I. Goryanin, W. J. Hedley, T. C. Hodgman, J.-H. Hofmeyr, P. J. Hunter, N. S. Juty, J. L. Kasberger, A. Kremling, U. Kummer, N. L. Novère, L. M. Loew, D. Lucio, P. Mendes, E. Minch, E. D. Mjolsness, Y. Nakayama, M. R. Nelson, P. F. Nielsen, T. Sakurada, J. C. Schaff, B. E. Shapiro, T. S. Shimizu, H. D. Spence, J. Stelling, K. Takahashi, M. Tomita, J. Wagner, and J. Wang, "The systems biology markup language (SBML): a medium for representation and exchange of biochemical network models," *Bioinformatics*, vol. 19, no. 4, pp. 524–531, Mar. 2003.
[21] A. Funahashi, Y. Matsuoka, A. Jouraku, M. Morohashi, N. Kikuchi, and H. Kitano, "CellDesigner 3.5: A Versatile Modeling Tool for Biochemical Networks," *Proc. IEEE*, vol. 96, no. 8, pp. 1254–1265, Aug. 2008.
[22] G. D. Lopaschuk, J. R. Ussher, C. D. L. Folmes, J. S. Jaswal, and W. C. Stanley, "Myocardial Fatty Acid Metabolism in Health and Disease," *Physiol. Rev.*, vol. 90, no. 1, pp. 207–258, Jan. 2010.
[23] D. A. Beard, "Modeling of Oxygen Transport and Cellular Energetics Explains Observations on In Vivo Cardiac Energy Metabolism," *PLoS Comput Biol*, vol. 2, no. 9, p. e107, Sep. 2006.
[24] Y. Kashiwaya, K. Sato, N. Tsuchiya, S. Thomas, D. A. Fell, R. L. Veech, and J. V. Passonneau, "Control of glucose utilization in working perfused rat heart.," *J. Biol. Chem.*, vol. 269, no. 41, pp. 25502–25514, Oct. 1994.
[25] D. Lagadic-Gossmann, K. J. Buckler, and R. D. Vaughan-Jones, "Role of bicarbonate in pH recovery from intracellular acidosis in the guinea-pig ventricular myocyte.," *J. Physiol.*, vol. 458, no. 1, pp. 361–384, Dec. 1992.
[26] P. Orlowski, M. Chappell, C. S. Park, V. Grau, and S. Payne, "Modelling of pH dynamics in brain cells after stroke," *Interface Focus*, vol. 1, no. 3, pp. 408–416, Mar. 2011.
[27] R. M. Denton, R. E. Yorke, and P. J. Randle, "Measurement of concentrations of metabolites in adipose tissue and effects of insulin, alloxan-diabetes and adrenaline," *Biochem. J.*, vol. 100, no. 2, pp. 407–419, Aug. 1966.
[28] V. Endeward, "The rate of the deoxygenation reaction limits myoglobin- and hemoglobin-facilitated O2 diffusion in cells," *J. Appl. Physiol.*, vol. 112, no. 9, pp. 1466–1473, May 2012.
[29] M. Cloutier, F. B. Bolger, J. P. Lowry, and P. Wellstead, "An integrative dynamic model of brain energy metabolism using in vivo neurochemical measurements," *J. Comput. Neurosci.*, vol. 27, no. 3, pp. 391–414, Dec. 2009.
[30] X. M. Wu, H. Gutfreund, S. Lakatos, and P. B. Chock, "Substrate channeling in glycolysis: a phantom phenomenon," *Proc. Natl. Acad. Sci.*, vol. 88, no. 2, pp. 497–501, Jan. 1991.

[31] P. Maliekal, T. Sokolova, D. Vertommen, M. Veiga-da-Cunha, and E. V. Schaftingen, "Molecular Identification of Mammalian Phosphopentomutase and Glucose-1,6-bisphosphate Synthase, Two Members of the α-D-Phosphohexomutase Family," *J. Biol. Chem.*, vol. 282, no. 44, pp. 31844–31851, Nov. 2007.

[32] L. J. Wong and I. A. Rose, "Kinetic competence of a phosphoryl enzyme intermediate in the glucose-1,6-p2 synthase-catalyzed reaction. Purification, properties, and kinetic studies.," *J. Biol. Chem.*, vol. 251, no. 18, pp. 5431–5439, Sep. 1976.

[33] A. M. Das and D. A. Harris, "Control of mitochondrial ATP synthase in heart cells: inactive to active transitions caused by beating or positive inotropic agents," *Cardiovasc. Res.*, vol. 24, no. 5, pp. 411–417, May 1990.

[34] D. F. Rolfe and G. C. Brown, "Cellular energy utilization and molecular origin of standard metabolic rate in mammals," *Physiol. Rev.*, vol. 77, no. 3, pp. 731–758, Jul. 1997.

[35] E. Murphy and C. Steenbergen, "Mechanisms Underlying Acute Protection from Cardiac Ischemia-Reperfusion Injury," *Physiol. Rev.*, vol. 88, no. 2, pp. 581–609, Apr. 2008.

[36] J. R. Neely and H. E. Morgan, "Relationship Between Carbohydrate and Lipid Metabolism and the Energy Balance of Heart Muscle," *Annu. Rev. Physiol.*, vol. 36, no. 1, pp. 413–459, 1974.

[37] A. S. Popel, "Theory of oxygen transport to tissue," *Crit. Rev. Biomed. Eng.*, vol. 17, no. 3, pp. 257–321, 1989.

[38] C. Seiler, M. Stoller, B. Pitt, and P. Meier, "The human coronary collateral circulation: development and clinical importance," *Eur. Heart J.*, p. eht195, Jun. 2013.

[39] J.-S. Kim, Y. Jin, and J. J. Lemasters, "Reactive oxygen species, but not Ca2+ overloading, trigger pH- and mitochondrial permeability transition-dependent death of adult rat myocytes after ischemia-reperfusion," *Am. J. Physiol. - Heart Circ. Physiol.*, vol. 290, no. 5, pp. H2024–H2034, May 2006.

[40] E. T. Chouchani, C. Methner, S. M. Nadtochiy, A. Logan, V. R. Pell, S. Ding, A. M. James, H. M. Cochemé, J. Reinhold, K. S. Lilley, L. Partridge, I. M. Fearnley, A. J. Robinson, R. C. Hartley, R. A. J. Smith, T. Krieg, P. S. Brookes, and M. P. Murphy, "Cardioprotection by S-nitrosation of a cysteine switch on mitochondrial complex I," *Nat. Med.*, vol. 19, no. 6, pp. 753–759, May 2013.

[41] J. P. French, J. C. Quindry, D. J. Falk, J. L. Staib, Y. Lee, K. K. W. Wang, and S. K. Powers, "Ischemia-reperfusion-induced calpain activation and SERCA2a degradation are attenuated by exercise training and calpain inhibition," *Am. J. Physiol. - Heart Circ. Physiol.*, vol. 290, no. 1, pp. H128–H136, Jan. 2006.

[42] K. Suzuki, B. Murtuza, I. A. Sammut, N. Latif, J. Jayakumar, R. T. Smolenski, Y. Kaneda, Y. Sawa, H. Matsuda, and M. H. Yacoub, "Heat Shock Protein 72 Enhances Manganese Superoxide Dismutase Activity During Myocardial Ischemia-Reperfusion Injury, Associated With Mitochondrial Protection and Apoptosis Reduction," *Circulation*, vol. 106, no. 12 suppl 1, pp. I–270–I–276, Sep. 2002.

[43] J. M. Schriewer, C. B. Peek, J. Bass, and P. T. Schumacker, "ROS-Mediated PARP Activity Undermines Mitochondrial Function After Permeability Transition Pore Opening During Myocardial Ischemia–Reperfusion," *J. Am. Heart Assoc.*, vol. 2, no. 2, p. e000159, Apr. 2013.

[44] P. H. Chan, "Role of Oxidants in Ischemic Brain Damage," *Stroke*, vol. 27, no. 6, pp. 1124–1129, Jun. 1996.

[45] N. S. Dhalla, A. B. Elmoselhi, T. Hata, and N. Makino, "Status of myocardial antioxidants in ischemia–reperfusion injury," *Cardiovasc. Res.*, vol. 47, no. 3, pp. 446–456, Aug. 2000.
[46] I. Fridovich, "Oxygen Toxicity in Prokaryotes: the Importance of Superoxide Dismutase," in *Superoxide dismutase*, vol. 1, 2 vols., L. W. Oberley, Ed. Boca Raton, Fla: CRC Press, 1982, pp. 79–88.
[47] R. S. Balaban, S. Nemoto, and T. Finkel, "Mitochondria, Oxidants, and Aging," *Cell*, vol. 120, no. 4, pp. 483–495, Feb. 2005.
[48] M. P. Murphy, "How mitochondria produce reactive oxygen species," *Biochem. J.*, vol. 417, no. 1, p. 1, Jan. 2009.
[49] J. F. Turrens, "Mitochondrial formation of reactive oxygen species," *J. Physiol.*, vol. 552, no. 2, pp. 335–344, Oct. 2003.
[50] B. Glancy and R. S. Balaban, "Role of Mitochondrial Ca^{2+} in the Regulation of Cellular Energetics," *Biochemistry (Mosc.)*, vol. 51, no. 14, pp. 2959–2973, Apr. 2012.
[51] K. Vinnakota, M. L. Kemp, and M. J. Kushmerick, "Dynamics of Muscle Glycogenolysis Modeled with pH Time Course Computation and pH-Dependent Reaction Equilibria and Enzyme Kinetics," *Biophys. J.*, vol. 91, no. 4, pp. 1264–1287, Aug. 2006.
[52] V. A. S. Ayyadurai and C. F. Dewey, "CytoSolve: A Scalable Computational Method for Dynamic Integration of Multiple Molecular Pathway Models," *Cell. Mol. Bioeng.*, vol. 4, no. 1, pp. 28–45, Oct. 2010.